JGR Solid Earth

RESEARCH ARTICLE
10.1029/2019JB017696

Hf and Nd Isotopic Constraints on Pre- and Syn-collisional Crustal Thickness of Southern Tibet

E. W. Alexander[1], M. M. Wielicki[1,2], T. M. Harrison[1], D. J. DePaolo[3], Z. D. Zhao[4], and D. C. Zhu[4]

[1]University of California, Los Angeles, CA, [2]University of Alabama, Tuscaloosa, AL, [3]University of California, Berkeley, CA, [4]China University of Geosciences, Beijing, China

Key Points:
- Geochemistry of Tibetan granitoids may serve as indirect proxies for crustal thickening processes throughout the India-Asia collision
- Whole-rock and zircon Lu-Hf isotopes are well-correlated in samples spanning ~180 Ma to ~20 Ma
- Geochemical proxies for depth of melt generation suggest a persistently thin crust at the southern margin of the Lhasa block until <50 Ma

Supporting Information:
- Supporting Information S1
- Table S1
- Table S2

Correspondence to:
E. W. Alexander,
ewalex@ucla.edu

Citation:
Alexander, E. W., Wielicki, M. M., Harrison, T. M., DePaolo, D. J., Zhao, Z. D., & Zhu, D. C. (2019). Hf and Nd Isotopic Constraints on Pre- and Syn-collisional Crustal Thickness of Southern Tibet. *Journal of Geophysical Research: Solid Earth*, *124*, 11,038–11,054. https://doi.org/10.1029/2019JB017696

Received 15 MAR 2019
Accepted 17 OCT 2019
Accepted article online 25 OCT 2019
Published online 16 NOV 2019

Abstract In Southern Tibet, voluminous granitoids emplaced between 225-20 Ma provide a spatiotemporal window into the geochemical and tectonic evolution of the crust. Hf and O isotope geochemistry of whole rocks and constituent zircons together with whole-rock chemistry reveal a coherent magmatic history of Gangdese granitoids, and by extension, crustal thickening history of S. Tibet. We observe a spatial isotopic gradient with N-S distance from the Indus-Tsangpo Suture (ITS), with younger, more ε_{Hf}-positive granitoids adjacent the ITS. Zircons range from $\varepsilon_{Hf} = -13$ to +11 in a broadly systematic fashion from north to south, generally independent of $^{206}Pb/^{238}U$ age. Adjacent to the ITS, syncollisional (<50 Ma) rocks have generally more heterogeneous ε_{Hf} than precollisional (>70 Ma) and early syncollisional (50-70 Ma) granitoids, likely reflecting increased assimilation of crustal material in syncollisional magmas as the crust thickened. Zircon $\delta^{18}O$ ranges between +4 and +8‰; syncollisional samples have exclusively mantle-like values (+5.5 to +6‰), with greater heterogeneity in precollisional samples. Zircon and whole-rock ε_{Hf} data reported here are consistent with previous Nd-based thermoisotopic models indicating that the Lhasa block maintained a wedge-shaped crustal geometry from the early Jurassic until the onset of collision. Given evidence of minimal post-50 Ma upper-crustal shortening, these results support earlier findings that the Tibetan crust reached its present ~75 km thickness via a roughly equal mixture of upper plate accretion and juvenile magmatic inflation on top of the ~30 km-thick of Indian crust underthrust beneath the Lhasa block.

Plain Language Summary Granites in what is now the Tibetan Plateau have formed continuously over the past 200 million years. The chemistry of these rocks, and the individual minerals inside them, contain information about the environment in which they formed. Zircon, an accessory mineral that is present in many types of igneous rocks, including these granites, is a time capsule of information about its formation: it contains radioactive elements that allow us to date the age of formation of the host rock as well as stable isotopes that can be used as proxies for the proportions of crustal and mantle parent material that the granites are made of. There are also trace elements in the whole rock that may provide information about the depth at which the granite formed. Our findings suggest that the southern margin of Tibet was thin from >200 million years ago until after the onset of the India-Asia continental collision approximately 50 million years ago, and the crust was thicker to the north well before the onset of collision. These findings provide a boundary the possible ways that the Lhasa block of Tibet may have accommodated the deformation induced by continental collision.

1. Introduction

More than 30 years after the classic tectonic models for the Tibetan-Himalayan orogen were formulated (Houseman et al., 1981; England & McKenzie, 1982; Tapponnier et al., 1982; England & Houseman, 1986), no direct test has yet been devised to reconstruct the crustal thickness of Southern Tibet prior to, during, or shortly after the onset of the India-Asia collision. The approximate magnitude of northward crustal shortening has been calculated to between 1800 and 2800 km depending on longitude (Johnson, 2002), but the exact mechanism of crustal thickening and the accommodation of deformation has been vigorously debated (England & Houseman, 1986; Ingalls et al., 2016; Kong et al., 1997; Kong & Bird, 1995; Peltzer & Saucier, 1996; Peltzer & Tapponnier, 1988). Neotectonic, structural and thermochronologic investigations provide useful proxies to understand the behavior of the Tibetan crust throughout collision (see Yin & Harrison, 2000), but indirect geochemical proxies toward a geographically broad understanding of crustal thickness in Tibet are emerging (e.g., Chen et al., 2018; DePaolo et al., 2019; Zhu et al., 2017). We seek to

expand this understanding by examining the crustal evolution of the southern portion of the Lhasa block through the lens of granitoid geochemistry and stable isotope systematics. We focus on Gangdese Batholith granites emplaced within ~100 km of the Indus-Tsangpo Suture (ITS), the boundary between India and Eurasia whose petrogenesis was shaped by the dynamic lower-crustal environment prior to and during collision (Ji et al., 2009; Zhu et al., 2011, 2015). The results we report here extend those described in DePaolo et al. (2019), which focused on Nd isotopic data and La/Yb. We report new zircon Hf and O isotope data, as well as whole-rock Hf and Nd data, from granitic and pre-batholithic rocks from a north-south transect near 92°E longitude. This work extends the isotopic data substantially farther east than those of DePaolo et al. (2019).

Isotopic signatures of magmatic rocks are governed by the composition of the primary melt source, as well as potential contribution from crustal material subsequently assimilated into the magma. Our interpretations emphasize the role of crustal assimilation in the genesis of granitic magmas, an issue which remains subject to debate (e.g. Chapman et al., 2017); a detailed discussion of the importance of crustal assimilation is given in DePaolo et al. (2019). The temperature of the country rock into which a magma intrudes is the most important limiting factor on the degree of assimilation between the juvenile melt and crustal material (Reiners et al., 1995). In general, cold crust is unlikely to be heated to anatexis by the injection of juvenile melt and thus the melt will not undergo significant alteration of its isotopic signature by assimilation of crustal material, while hot crust will be more readily available for assimilation. When the assimilation rate competes with the rate at which fractional crystallization is occurring, there can be a large crustal contribution to the isotopic signature (DePaolo, 1981; Spera & Bohrson, 2002). Storage at high temperature, whether due to high country rock initial temperature or periodic magma recharge, will result in greater total assimilation and thus a more crustal-like isotopic signature (DePaolo, 1981; Reiners et al., 1995). We proceed on the assumption that higher degrees of assimilation are associated with higher wall-rock temperature and that the majority of melt hybridization occurs at or near the Moho (DePaolo, 1981; DePaolo et al., 2019; Klaver et al., 2018; Rapp et al., 2003; Reiners et al., 1995).

While steady-state magma flux and assimilation cannot be assumed for upper-crustal volcanic systems, in which a large quantity of low-crystallinity magma must be generated prior to eruption (DePaolo et al., 2019; Simon et al., 2014), granitic batholiths are commonly characterized by episodic growth and zircon crystallization histories spanning 10^5 to 10^6 years (McNulty et al., 2000; Walker et al., 2007; Wiebe & Collins, 1998). Accordingly, typical granitoids form from low magma flux, with the ratio of assimilation rate and recharge rate only slightly lower than steady state. The "Temperature-Flux" model developed by DePaolo et al. (1992, 2019) defines the "Neodymium Crustal Index" (NCI), which relates the whole-rock ε_{Nd} of a pluton to the ε_{Nd} of recharging magma and assimilated (crustal) material, can be used to approximate Moho temperature, and therefore depth, as a function of the pluton's degree of crustal assimilation. DePaolo et al. (2019) use model parameters based on calibrated isotopic studies of layered intrusions (Hammersley & DePaolo, 2006). In open systems it is difficult to constrain the validity of Temperature-Flux model parameters; factors such as cooling rate, pluton volume, and crystallization rate necessarily change during recharge and assimilation in an evolving magma body. The use of this model to reconstruct crustal thickness relies on several assumptions, the most important being the geothermal gradient of the system. The crustal thickness is derived from the calculated Moho temperature and the assumed geothermal gradient; while the paleo-geotherm of Southern Tibet has not been directly reconstructed, other continental arcs have a relatively shallow geothermal gradient in the mid- to lower-crust, consistent with the model geotherm used by DePaolo et al. (2019) (Rothstein & Manning, 2003). Other assumed parameters, including those that address rate of crystallization DePaolo et al. (2019) further demonstrated with a Monte Carlo simulation that the model is relatively robust at predicting NCI and Moho temperature with variation of unconstrained parameters within a geophysically reasonable range.

In this study, we adapt the Temperature-Flux model to the Hf isotopic variation in pre- and syn-collisional granitic zircons, which are resistant to secondary alteration or addition of radiogenic Hf. The Lu-Hf isotopic system behaves similarly to Sm-Nd; the distribution coefficient ratio during partial melting D_{Lu}/D_{Hf} is approximately twice that of D_{Sm}/D_{Nd}, resulting in greater radiogenic enrichments or depletions of Hf isotopes relative to Nd in derived magmas. Thus, the Lu-Hf system magnifies differential evolution of DM and crustal $^{176}Hf/^{177}Hf$ relative to Sm-Nd. Modern DM is characterized by a maximum $\varepsilon_{Hf} \approx +18$

(Vervoort & Blichert-Toft, 1999, and references therein). As with Nd, the average ε_{Hf} of continental material is dependent on the timing of fractionation of crustal material from DM. Reconstructing crustal evolution using Hf requires a temporal anchor to which isotopic data may be attached. Zircon ($ZrSiO_4$) has proved ideal for constraining not only the age of magmatic rocks of a wide variety of compositions, but also as a record of the thermal history and isotopic signature of its source magma (Harrison et al., 2014). Zircon typically incorporates up to 1-2 wt% Hf and is characterized by extremely low Lu/Hf (< 0.0005) (Finch & Hanchar, 2003; Kinny & Maas, 2003). The $^{176}Lu/^{177}Hf$ in zircon at the time of crystallization therefore is sufficiently low as to have a negligible and easily corrected contribution to the final $^{176}Hf/^{177}Hf$ of the crystal. The $^{176}Hf/^{177}Hf$ of the source melt from which the zircon crystallized is preserved, permitting reconstruction of crustal differentiation and magmatic assimilation processes when combined with zircon U-Pb age. Relating zircon isotopic composition to bulk-melt assimilation processes requires an understanding of the link between the thermal history of a pluton – which relates to its ability to crystallize zircon – and the degree of assimilation possible within the constraints of that thermal history. Prolonged recharge will suppress crystallization and lead to a broader range of isotopic compositions of the melt during the period that zircon is crystallizing, resulting in an isotopically heterogeneous population of zircon within a single pluton (Lovera et al., 2015). Plutons with a high zircon ε_{Hf} MSWD are not suitable for the Temperature-Flux model due to the complicating effects of extensive magma recharge on the relationship between ambient crustal temperature and assimilation.

To calculate a "Hafnium Crustal Index" (HCI) requires estimates of both the mantle and crustal endmember components that contribute to the formation of granitic magma. The majority of Lhasa block zircon ε_{Hf} reported by Zhu et al. (2011) are consistent with a broadly Proterozoic crustal model age of the southern Lhasa terrane (i.e. average crustal $\varepsilon_{Hf} \approx -15$), with some grains inherited from Archean crust, assuming a source $^{176}Lu/^{177}Hf = 0.015$. Results of Hf and Nd isotopic compositions of pre-batholithic metasedimentary rocks presented here allow us to refine our estimate of crustal ε_{Hf} for the southern Tibetan basement rocks that predate the Mesozoic to Cenozoic granitoids (see discussion).

Interpreting magmatic mixing and assimilation histories from radiogenic isotopes can lead to mistaken assumptions about provenance, as a mixing relationship between juvenile mantle and ancient crust cannot be distinguished a priori from anatexis of old and fractionated mantle-derived material, such as lower-crustal cumulates. Oxygen isotopes are independent of crustal age, and whole-rock $\delta^{18}O$ of magmatic rocks is directly derived from the source material, whether that be the DM ($\delta^{18}O = +5.5‰$; Ito et al., 1987) or supracrustal material (from +15‰, for hydrothermally altered MORB, up to +42‰ for pelagic clays; Eiler, 2001), or some combination thereof. Oxygen isotopes in zircon record the magmatic signature at the time of crystallization – with an approximate -2‰ ^{18}O(zircon-whole rock) – and have been shown to be resistant to resetting due to hydrothermal or deuteric alteration relative to other minerals (Bindeman, 2008; King et al., 1997; Trail et al., 2009; Valley, 2003). The diffusive lengthscale of ^{18}O in zircon is ~1 μm/Ma at 500°C and ~275 μm/Ma at 900°C under hydrothermal conditions (Watson & Cherniak, 1997), making zircon reasonably retentive of its most recent magmatic conditions, and more resistant to subsolidus alteration than other minerals. Petrographic and geochemical evidence shows Gangdese batholith granitoids have all undergone some degree of hydrothermal or deuteric alteration (Blattner et al., 2002; Zhang et al., 2015). As long as care is taken to avoid zircons whose intra-sample oxygen isotope heterogeneity suggest secondary mixing with a hydrothermal or meteoric water source, zircon will provide the most robust mineral record of the primary magmatic oxygen isotope signature in these rocks. In this study we explore the multiple uses of zircon as a geochemical time capsule to explore the spatiotemporal crustal evolution of Southern Tibet throughout the India-Asia collision.

2. Materials and Methods

Granitoid samples used in this study were collected during numerous field trips between 1994 and 2014. Sample locations are depicted in Figure 1, with corresponding numbers listed in Table S1. Whole-rock major and trace element analyses were either performed at Pomona College on a 3.0 kW Panalytical Axios wavelength-dispersive XRF spectrometer or taken from Harrison et al. (2000). Pulverized samples were prepared with a 2:1 ratio of dilithium tetraborate and rock powder, which was then fused at 1000°C for 10 minutes, reground and fused again, and polished on diamond laps prior to analysis. Concentrations were

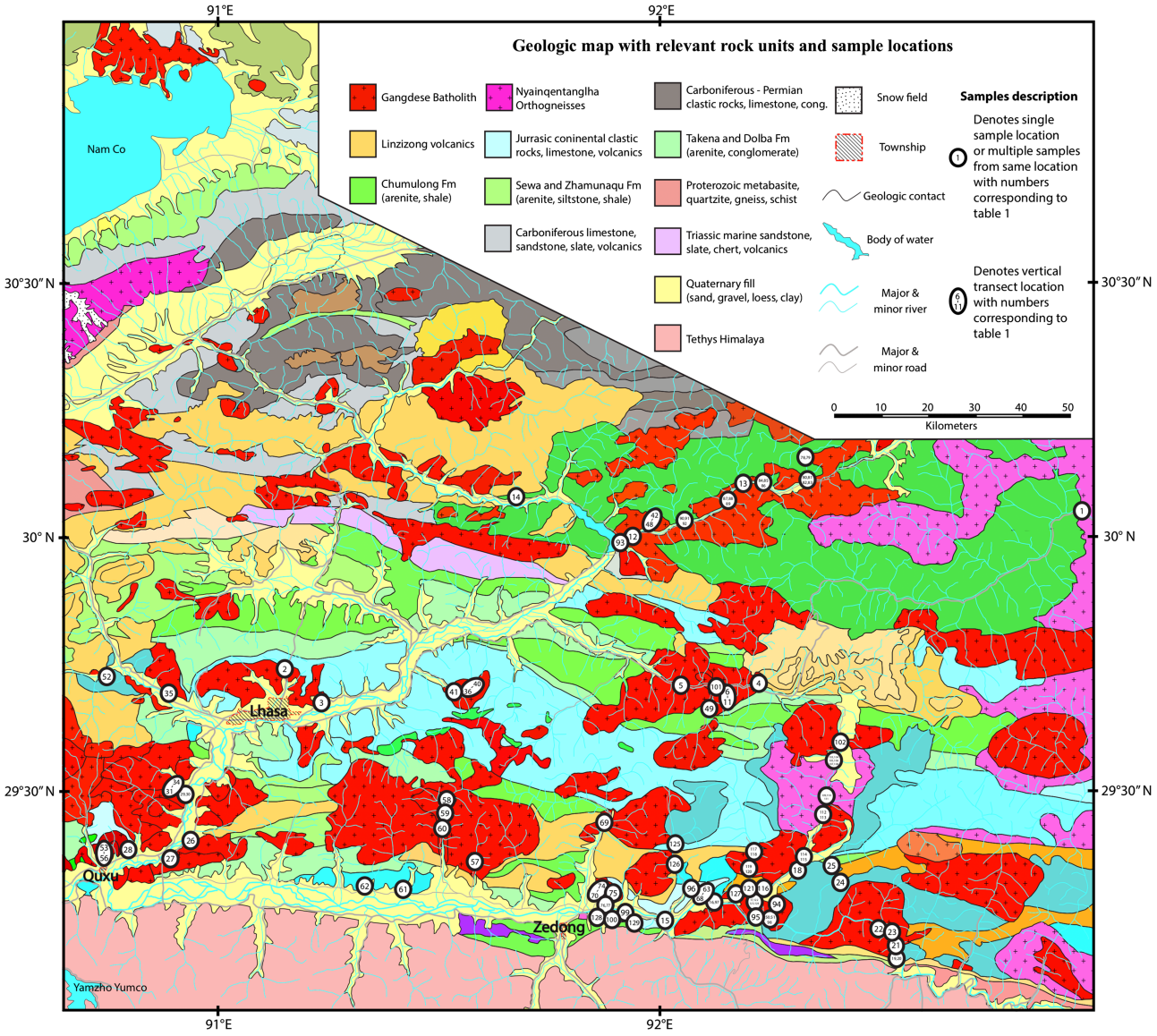

Figure 1. Map of sample locations; numbers corresponding to sample names and data are listed in Table S1. In cases where multiple sample numbers are listed within a symbol, the sample locations were closer together than the diameter of the symbol.

determined using reference calibration curves using 55 certified reference materials. See Johnson et al. (1999) and Lackey et al. (2012) for detailed methodology and error assessment.

Zircon grains were separated from a crushed and sieved portion of each rock and mounted in epoxy, along with age and Hf standard material for internal reproducibility, and the surface of the grain mounts were polished flat. Mounts were coated with a ~100 Å layer of Au for SIMS measurements. Each grain was analyzed simultaneously for U-Pb age and Ti concentration on a CAMECA *ims*1270 at UCLA, using a 10-15 nA primary O^- beam. U-Pb age standard AS3 (1099±1 Ma; Paces & Miller, 1993) was used for the U-Pb age calibration, and NIST SRM-610 glass (Jochum et al., 2011) and AS3 (Aikman, 2007) were used to standardize Ti concentration. In separate sessions, the same zircons were analyzed on the CAMECA *ims*1270 at UCLA for $^{18}O/^{16}O$ using a 4 nA primary Cs^+ beam in multicollection mode, with a mass resolving power of over 4000. Grains were analyzed in 12 cycles with 10 seconds each of counting time, with 1 second of waiting time between cycles. Zircon standards AS3 ($\delta^{18}O$ = +5.34‰, Trail et al., 2007) and 91500 ($\delta^{18}O$ = +9.86‰; Wiedenbeck et al., 2004) were used, with 91500 used for tuning and AS3 grains on each mount for isotopic calibration (see Mojzsis et al., 2001 and Booth et al., 2005, for details).

In situ zircon Lu-Hf measurements were made with a 193-nm excimer laser coupled to a ThermoFinnigan Neptune MC-ICPMS at UCLA. Zircons were analyzed in their original epoxy mounts using apertures with nominal laser spot diameters of 52 and 69 μm, with zircon standards Mud Tank, Monastery, and Temora (Woodhead & Hergt, 2005) as well as AS3 (Harrison et al., 2008). The in-situ LA-ICPMS method has insufficient mass resolving power to separate isobaric interferences on Hf at masses 174 and 176. Yb, which is present in trace levels in zircon (Finch & Hanchar, 2003), interferes on both 174 and 176; Lu, while generally in low abundance in zircon (Patchett et al., 1982), interferes on mass 176. The correction on masses 174 and 176 is achieved by measuring non-interfering Yb and Lu masses and calculating the contribution of the interfering masses to the 174 and 176 peaks using natural isotopic abundances. Contamination from cracks or inclusions is monitored with ^{181}Ta, though it was never detected above baseline in these measurements. Masses ^{171}Yb, ^{173}Yb, ^{174}Hf, ^{175}Lu, ^{176}Hf, ^{177}Hf, ^{178}Hf, ^{179}Hf, and ^{181}Ta were measured in 15 cycles per analysis, with a blank run for baseline correction between each block. For each sample, 6-10 grains were analyzed to account for individual grain heterogeneities due to inherited igneous cores or multi-stage growth histories. Data were corrected using the peak-stripping procedures detailed in Bell et al. (2011).

Finely pulverized whole-rock samples were analyzed for Hf isotopes at the PCIGR labs at the University of British Columbia. Aliquots of 100 mg of each sample was dissolved using high-pressure acid digestion in PTFE bombs. Hf was separated by column chemistry and analyzed by static MC-ICP-MS for masses 180, 179, 178, 177, 176 and 174 with monitoring of ^{176}Lu and ^{172}Yb; results are corrected for ^{176}Lu, ^{176}Yb, and ^{174}Yb interferences using natural abundances corrected for instrumental mass fractionation (see Weis et al., 2007 for details).

The zircon crystallization temperature (T_{zir}) was calculated using the Ti-in-zircon thermometer calibration of Ferry and Watson (2007). The concentration of Ti in zircon is given by:

$$\log\left(ppm\ Ti\right) = (5.711 \pm 0.072) - \frac{4800 \pm 86}{T(K)} - \log a_{SiO_2} + \log a_{TiO_2}$$

The inclusion of $\boldsymbol{a_{TiO_2}}$permits expansion of the thermometer's utility to rutile-undersaturated systems; $\boldsymbol{a_{SiO_2}} \approx \mathbf{1}$ was found to be appropriate not only for natural systems whose mineral assemblages imply silica saturation, but also for experimental run products with unbuffered $\boldsymbol{a_{SiO_2}}$. The uncertainty in the linear fit to the experimental data results in an uncertainty in calculated T of ±12°C (2σ); uncertainty in Ti concentration added ±11° to ±40° (1σ) to the temperature estimates. The activity of rutile in the system, $\boldsymbol{a_{TiO_2}}$, is necessary for the temperature calculation but is difficult to precisely constrain in granitic systems. As the whole rock chemistry is not a good proxy for $\boldsymbol{a_{TiO_2}}$ in granitic rocks, we estimate $\boldsymbol{a_{TiO_2}}$based on the assemblage of Ti-bearing minerals in the granites of interest. We use $\boldsymbol{a_{TiO_2}} = 0.6$ due to the absence of rutile (TiO_2), and presence of sphene ($CaTiSiO_5$) and ilmenite ($FeTiO_3$), in the majority of Gangdese Batholith granitoids, which implies $0.6 < \boldsymbol{a_{TiO_2}} < 0.9$ (Kapp et al., 2009). The potential error induced by underestimation of $\boldsymbol{a_{TiO_2}}$averages 46°C for maximum $\boldsymbol{a_{TiO_2}} = 1.0$; 36°C for maximum $\boldsymbol{a_{TiO_2}} = 0.9$.

3. Results

Granitoid ^{206}Pb/^{238}U ages, locations, zircon Ti, T_{zir}, and major element data are reported in supplementary material (SM) Table S1. Whole-rock ε_{Nd} and ε_{Hf}, zircon ε_{Hf} and δ^{18}O, sample latitudes, and U-Pb ages (where available) are reported in SM Table S2.

3.1. U-Pb Ages of Southern Lhasa Block Granitoids

The zircon ^{206}Pb/^{238}U ages of granitoids in this study show a similar age distribution to previous work on Lhasa block granitoids (Figure 2) (Harrison et al., 2000; Quidelleur et al., 1997; Zhu et al., 2009, 2011, 2015). Geochronological datasets such as these are generally incomplete, as sample collection cannot perfectly account for every unit and weight the number of analyses appropriately based on volumetric abundance of discrete plutons. Units found in or near roadcuts or otherwise accessible areas will tend to be overrepresented relative to more inaccessible outcrops. Apparent gaps or spikes in magmatism must therefore be regarded skeptically, especially in an intrusive magmatic complex as expansive as the Gangdese batholith; we therefore abstain from interpreting the absolute quantity of ages for various age brackets as "spikes" in magmatism. While there is a general trend of youngest granites clustered nearest to the ITS,

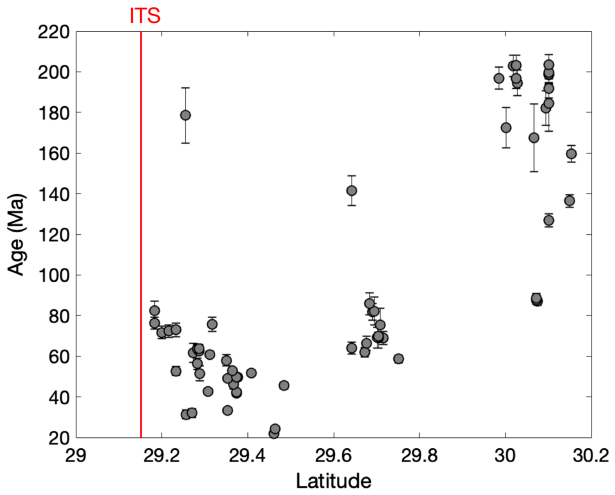

Figure 2. North-South distribution of sample ages; error bars are 2 s.e.; the red line is the modern latitude of the Indus-Tsangpo suture (ITS) at 92°E.

and oldest >75 km north of the suture, there are precollisional samples (up to 180 Ma) adjacent to the ITS (Figure 2). Younger granodiorite units may exist in the subsurface further north; young (~10 Ma) two-mica granites have been reported ~100 km north of the ITS (DePaolo et al., 2019) but are not found in our dataset. Syncollisional (<50 Ma) granites are found exclusively within ~40 km of the ITS in our study, consistent with previously reported Tertiary granitoids found in abundance near the ITS and relatively sparse to the north (e.g. Harrison et al., 2000; Mo et al., 2005; Yin & Harrison, 2000; Zhu et al., 2015, 2011). We define "precollisional" rocks as those with zircon U-Pb ages >70 Ma, and "early syn-collisional" rocks as 50-70 Ma according to maximum and minimum estimates of the onset of collision between ~65 and ~50 Ma (Le Fort, 1996; Rowley, 1996; Yin & Harrison, 2000).

3.2. Hf Isotopes of Pre-Batholithic Metasedimentary Rocks

Figure 3 shows results for southern Lhasa block metasedimentary rocks and granitoids in the region between 89.5 and 92.5°E. The schist ε_{Nd} values fall between -9 and -12; this is consistent with the range used by DePaolo et al. (2019) for the crustal endmember in the Nd isotope Temperature-Flux model. Figure 4 shows the relationship between zircon ε_{Hf}, granitoid whole-rock ε_{Nd}, and the pre-batholithic endmembers. In the region north of 29.8°N, there are 2-mica granites with $\varepsilon_{Nd} \approx$ -12 to -14, so the crustal component north of 29.8° must have slightly lower ε_{Nd}. The same schist samples show a range of ε_{Hf} values from -3 to -23, with the discontinuity shifted south to ~29.6°N. Previously reported Mesozoic granites from ~ 30°N have ε_{Hf} in the range -12 to -16, so it is likely that the ε_{Hf} value of the crust is closer $\varepsilon_{Hf} \leq$ -17, consistent with our results for schists north of 29.6°N. South of 29.6°N, the data are consistent with crustal $\varepsilon_{Hf} \approx$ -10. Previous compilations of granitoid zircon and whole-rock ε_{Hf} data from the southern Lhasa block, including those from Paleozoic granitic gneisses, suggest that the pre-Mesozoic crust south of 29.6°N had ε_{Hf} values in the range of -5 to -10, consistent with these new data (Chapman & Kapp, 2017; Zhu et al., 2011). One of the metasediments analyzed is a metavolcanic sample with $\varepsilon_{Hf} \approx +13$, consistent with a mantle endmember $\varepsilon_{Hf} \approx +18$ used in our Hf isotope Temperature-Flux model (see discussion).

3.3. Zircon Hf Isotopes

There is good correlation between whole-rock ε_{Hf} and zircon ε_{Hf}, independent of unit age (Figure 5a) such that we are confident that the zircon ε_{Hf} can be used as a proxy for the whole-rock signal. The relationship is quantified by least squares-maximum likelihood regression (after York et al., 2004), with slope $b = 0.97 \pm 0.21$ and intercept $a = 0.85 \pm 1.1$; error 1 σ. Cases where zircon ε_{Hf} is markedly more positive than the whole rock ε_{Hf} – indicative of isotopic disequilibrium between zircons and their host rocks – are associated with high whole-rock SiO_2 (>75%) (Figure 5b), typically have T_{zir} below the hydrous granite solidus, and high MSWD in zircon O and/or Hf isotopes (Table S1). These factors may indicate that the zircon was always saturated at magmatic conditions, and the Hf isotopic composition of inherited or restitic zircon was preserved rather than crystallizing new zircon. The youngest plutons, <50 Ma, show substantially more variable zircon ε_{Hf}, compared to >50 Ma samples, and a strong correlation between zircon ε_{Hf} and whole rock ε_{Hf}.

While in situ analysis for zircon Hf isotopes using LA-ICP-MS provides improved spatial resolution compared to solution methods, the relatively large laser spot size necessary for adequate sensitivity introduces uncertainty due to the likely averaging of multiple growth domains. In many zircon grains, especially those with inherited cores or long-lived, multi-stage magmatic growth histories, LA-ICP-MS analyses will average multiple discrete zones which may represent a wide range of crystallization conditions. This concern is partly addressed by analyzing multiple grains from each sample and interpreting the distribution of isotopic values and ages among the population. The isotopic composition of grains with substantial age inheritance (>20% difference) is not included in the computed weighted mean sample values, as the signal is not representative of final crystallization conditions. Excluding inheritance, inter-grain heterogeneity was typically within 2σ of analytical error for each sample; paired with good correlation between zircon ε_{Hf} and whole-rock ε_{Hf}, spatial averaging from laser ablation has a minimal effect on the results. Overall MSWD values

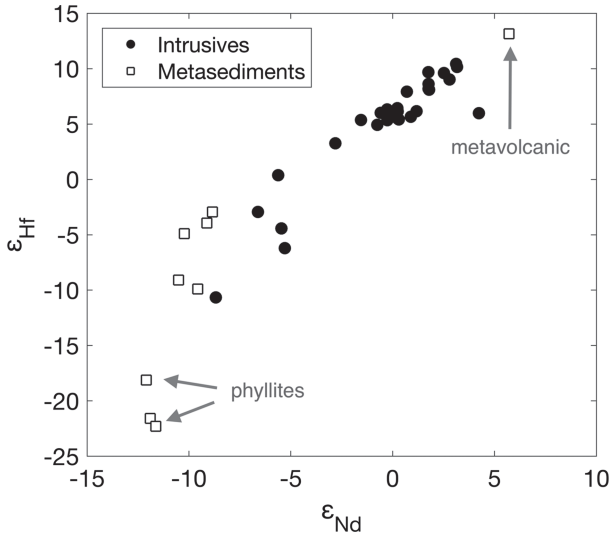

Figure 3. Whole-rock ε_{Nd} and ε_{Hf} of pre-batholithic metasedimentary rocks as well as granitoid intrusive and hypabyssal rocks. The metavolcanic sample, with ε_{Nd} = +5.7 and ε_{Hf} = +13.2, is consistent with a DM-like juvenile mantle endmember; crustal phyllites with ε_{Nd} = -8 to -12 and ε_{Hf} = -9 to -20 show a likely crustal endmember of $\varepsilon_{Nd} \approx$ -8 to -12 and $\varepsilon_{Hf} \approx$ -10 to -20; both increase with latitude.

for zircon ε_{Hf} have a median of 0.72, with a relatively broad distribution ($1\sigma_{MSWD}$ = 4.8); anomalously low MSWD for some populations likely reflect the overestimation of analytical error from counting statistics. Cases with high MSWD with a small number of outliers in individual grain analyses could be spurious variation in ε_{Hf}, which can result from ablation of restitic inclusions or other inherited material which may not have been caught by our age inheritance filter. High MSWD relating to an overall broad inter-grain distribution of ε_{Hf} could reflect the effects of prolonged magma recharge during zircon crystallization (Lovera et al., 2015; see introduction).

3.4. Zircon Ti Thermometry

Zircon Ti analyses have analytical errors of <1 to 4 ppm. Calculated T_{zir} for Lhasa block granitoids ranges between 620±28°C and 924±35°C; maximum and minimum values occur at 65.9 and 60.9 Ma, respectively (Figure 6). As many as 22% of all samples have T_{zir} below the hydrous granite solidus (ca. 620°C), which is either due to overestimation of a_{TiO_2}, which leads to underestimation of temperature, or due to subsolidus zircon crystallization, likely in a fluid-rich, undercooled stage of pluton solidification. Total error in T_{zir} induced by the uncertainties in calibration, analytical Ti measurements, and estimation of a_{TiO_2}, can lead to 4-5% uncertainty in temperature. The total range of calculated temperatures far exceeds variation induced by uncertainty, so broad trends in the distribution of T_{zir} can still be resolved.

3.5. Zircon Oxygen Isotopes

Oxygen isotope results are reported using standard delta notation relative to Vienna Standard Mean Ocean Water (VSMOW); error is reported at one standard deviation. The average $\delta^{18}O$ value for all samples irrespective of age was 5.77±0.80‰ (1σ of total distribution), with average analytical error of 0.34‰. Syncollisional samples (U-Pb age ≤ 70 Ma) have mean $\delta^{18}O$ = 5.59±0.77‰ (1σ). Median MSWD of oxygen values is 2.6, with some anomalously high values derived from greater intra-sample heterogeneity. There is no obvious correlation between age and $\delta^{18}O$; there is greater heterogeneity in >100 Ma samples, possibly due to inheritance, increased geographic distribution, or higher occurrence of secondary alteration. There is additionally minimal correlation with zircon ε_{Hf} (Figure 7) and no correlation with T_{zir}.

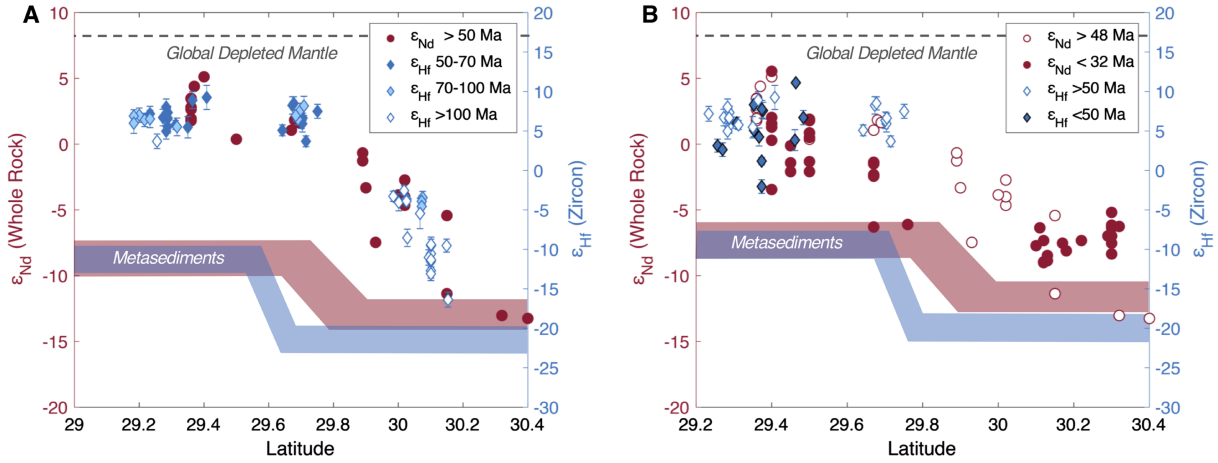

Figure 4. Zircon ε_{Hf} (blue, this study) and whole-rock ε_{Nd} (red, DePaolo et al., 2019) of pre- and early syn-collisional samples (A) as well as later syn-collisional samples (B) versus latitude. Red symbols correspond to left axis; blue to right axis. Shaded fields show likely crustal assimilant endmembers for Nd (red) and Hf (blue); Nd endmember becomes more positive for <32 Ma samples (DePaolo et al., 2019). Error bars on ε_{Hf} are 2 s.e.; dashed lines represent isotopic values for global average DM (ε_{Hf} = +18; ε_{Nd} = +8). Vertical axes are scaled to match both the global DM and crustal endmember values.

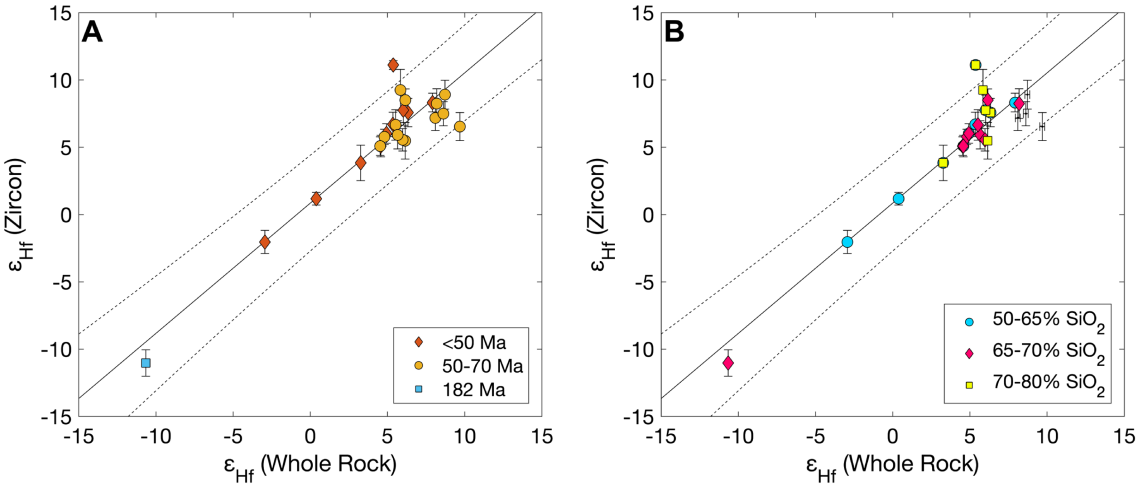

Figure 5. Whole-rock and zircon ε_{Hf} values according to age (a) and whole-rock weight percent SiO_2 (b). Error bars for zircon ε_{Hf} is 2 s.e.; error bars for whole-rock ε_{Hf} are narrower than the data markers. Black solid line is the least squares-maximum likelihood fit (after York et al., 2004) described by $\varepsilon_{Hf(z)} = (0.968\pm0.207)\varepsilon_{Hf(wr)} + (0.850\pm1.05)$, MSWD = 2.86; black dashed lines are the 95% confidence bounds of the linear fit.

4. Discussion

4.1. Assimilation Evidence

While magmatic inflation may account for ~15 km of Tibetan crustal thickening throughout collision (Chen et al., 2018; DePaolo et al., 2019; Mo et al., 2007), magmatic heat added to the crust is insignificant compared to total orogenic heat flow, and therefore cannot explain increased assimilation (De Yoreo et al., 1989). Magma recharge, as opposed to increased crustal thickness (i.e. higher wall-rock temperature), could promote heterogeneity of zircon ε_{Hf} based on results of RAFC modeling of ε_{Hf} in zircon (Lovera et al., 2015). Prolonged recharge increases the crystallization window of zircon, allowing zircon to record the prolonged assimilation process induced by recharge. The current analytical restrictions that generally limit zircon ε_{Hf} measurements to a single datum per grain precludes resolving depth-dependent Hf isotopic variations that could reveal complex thermoisotopic histories in individual zircons. However, inter-grain heterogeneity of ε_{Hf} in magmatic zircons within each sample can provide a sense of overall zircon ε_{Hf} heterogeneity. The inter-grain zircon ε_{Hf} variability for individual samples of Lhasa-block syncollisional plutons reported here are within analytical error, so inter-sample heterogeneity among <50 Ma plutons cannot be explained by an increase in magma recharge alone. Increased assimilation from higher wall-rock temperature at the base of a thicker crust is most consistent with a greater crustal component in the zircon ε_{Hf} of syncollisional granitoids. The similar spatial trends of whole-rock ε_{Nd} and zircon ε_{Hf} (Figure 4) suggest that where assimilation occurred, thermal and chemical conditions were such that there was moderate to low discrimination between Nd and Hf isotopic assimilation mechanisms, even in cases where both zircon and whole rock retained a relatively mantle-like signature in both systems.

Hf crustal model age estimates for the Lhasa block range between 1.5-3.0 Ga based on central- to northern-Lhasa inherited zircon ages and Hf isotopes (Zhu et al., 2011). Mantle-like $\delta^{18}O$ values for all but a few early-Jurassic samples indicate the crustal assimilant is likely ≥1.5 Ga mantle-derived rock, rather than isotopically evolved supracrustal material, which additionally supports our interpretation that granite hybridization proceeds mostly at the base of the crust. $\delta^{18}O$ values for all samples are within ±2‰ of the average mantle value $\delta^{18}O$ = +5.5‰ (Ito et al., 1987), which is substantially less enriched than the minimum $\delta^{18}O$ values expected for metasedimentary material. As zircon $\delta^{18}O$ is unlikely to be increased by secondary processes (King et al., 1997), values that are more negative than average mantle are consistent with lower-crustal gabbros, which range from +3.5‰ to +5.5‰, or interactions with meteoric water (Eiler, 2001; Gregory & Taylor, 1981). Moreover, samples with $\delta^{18}O$ lower than average mantle do not show signs of heterogeneity that would be expected from partial resetting (average MSWD of this subset is no greater than the data in aggregate). Granitoid samples (>55% SiO_2) range in aluminosity, with molar $Al_2O_3/(CaO+Na_2O+K_2O)$ from 0.74 to 1.19 (Figure 8). Major element trends are broadly consistent with fractional

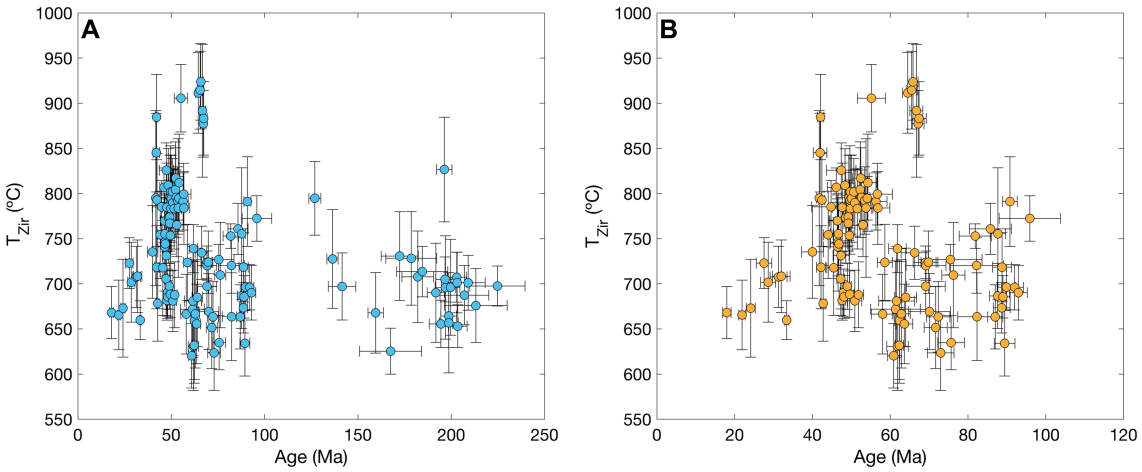

Figure 6. Ti-in-zircon temperatures and ages of all samples (A) and samples up to 100 Ma (B), calculated using the calibration of Ferry and Watson (2007). Age error bars are 2 s.e.; T_{zir} error bars include the 1σ analytical uncertainty in Ti concentration as well as the uncertainty of the thermometer calibration at the 95% confidence level. For all samples, $a_{TiO_2} = 0.6$ and $a_{SiO_2} = 1$ was used.

crystallization (Figure 8; supplemental Figure S1); assimilation would have had to occur with a protolith whose major element ratios were not substantially different from the juvenile melt.

The origin of mafic melts that contribute to granitic magmatism impacts the isotopic and chemical signature of the resultant granitoids; the most plausible source of a basaltic endmember melt must be evaluated in the context of the isotopic and geochemical data presented here. Partial melting and assimilation of eclogite with a hydrous basalt in arc settings has been shown to produce granitic melt in equilibrium with the eclogite residue (Bouilhol et al., 2015; Rapp et al., 2003). Continual production of slab-derived melts with an eclogitic restite is a tempting explanation for the production of these melts and would not require substantial juvenile DM component in the melts to produce relatively radiogenic Hf isotopes. However, partial melts of slab materials would have more positive $\delta^{18}O$ due to the incorporation of altered basaltic crust; only 100% slab melt could produce a mantle-like $\delta^{18}O$ with no juvenile component, and there would be no eclogitic restite (Eiler, 2001). Thermodynamic modeling of subduction zone melting further suggests that slab dehydration occurs at much shallower pressures than slab melting, and the fluids released during dehydration can produce substantial melting of a thick, hydrated mantle wedge (Bouilhol et al., 2015). This melt then readily travels to the base of the overriding plate and fractionates, potentially without removal of garnet or amphibole, leading to an "adakitic" signature in some fractionated products. Depending on the depth of fractionation, if garnet and amphibole are removed, the same primary melting process (melting of a hydrated mantle wedge) may produce both adakitic and calc-alkaline felsic products. This process may provide an explanation for the appearance of a range of adakitic signature in syncollisional magmas, which have previously been attributed to geodynamically disfavored processes such as "slab breakoff" (e.g. Chung et al., 2005; Chen et al., 2014; Zhu et al., 2017; cf. Garzanti et al., 2018), or have been used to imply cessation of calc-alkaline Gangdese arc magmatism by 45 Ma (e.g. Ji et al., 2016) – which is clearly not the case based on the persistence of calc-alkaline melts well after 45 Ma, as presented here (Figures. 2, 8).

Fractional crystallization of a pure mantle melt is more favored by the major element relationships seen in <70 Ma granites across the Lhasa block (Figure 8). If these granites were derived from a pure DM source, however, they would be expected to have exclusively mantle-signature $\varepsilon_{Hf} \approx +18$ and $\delta^{18}O \approx +5.5$ (Ito et al., 1987; Vervoort & Blichert-Toft, 1999), as isotopic ratios cannot be altered by closed-system magmatic fractionation. What we observe in early- and later-syncollisional granites is an ε_{Hf} signature that is moderately depressed relative to DM, and an average $\delta^{18}O$ that is slightly elevated relative to average DM value (Figure 7). Nd isotopes additionally demonstrate an isotopic mixing trend that favors large fractions of mantle melt mixed with some assimilated crustal material (DePaolo et al., 2019). Intermediate values of ε_{Hf} are interpreted as the result of assimilation between juvenile mantle-derived melt (DM, $\varepsilon_{Hf} \approx +18$) and less radiogenic basement rocks of the Lhasa block (ε_{Hf} -5 to -20). The bulk of assimilation is assumed to occur at or near the Moho, where the temperature contrast between juvenile magma and surrounding lower-

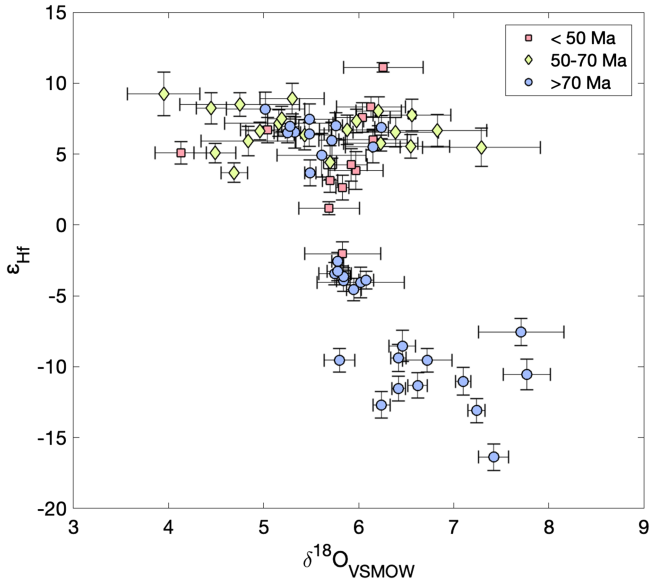

Figure 7. Zircon ε_{Hf} and $\delta^{18}O_{VSMOW}$ (Vienna Standard Mean Ocean Water); error bars are 2 s.e. The >70 Ma group ranges relatively continuously in age up to the oldest at 203.5±5 Ma.

crustal rocks is small, favoring higher assimilation. While additional assimilation may occur following fractionation and emplacement of granitic melts, the necessarily lower magmatic temperature and greater polymerization of a silicic melt would lower the diffusivity of rare earths in the melt (Mungall et al., 1999); and low-T wallrock would minimize the ability of the melt to extract substantial crustal material. The fractionation of melt sourced from DM, and possibly assimilated with eclogitic residue, additionally requires that hybridization and fractionation occur at the base of the crust.

4.2. Isotopic Constraints on Crustal Thickness

The granitoids along the 92° E traverse provide a window into the plutonic evolution of the southern Lhasa block: this area provides a near-continuous plutonic history from <20 Ma to ca. 225 Ma (Figure 2), as greater exhumation of the eastern Lhasa block has exposed younger (syncollisional) plutons (Harrison et al., 1992; Zhu et al., 2015). For any given age range of Gangdese granitoids within the Lhasa block, east-west variation in geochemistry and age distributions is less significant relative to the substantial variation associated with northward distance from the southern margin of Eurasia, at the Indus-Tsangpo Suture (ITS) (Chen et al., 2014; Chung et al., 2009; Harrison et al., 2000; Kapp et al., 2005; Yin & Harrison, 2000; Zhu et al., 2011). We therefore consider north-south distance from the ITS to be the main variable in spatial isotopic trends.

We interpret our results through the lens of the thermoisotopic framework developed by DePaolo et al. (1992) and quantified with respect to the Tibetan granites by DePaolo et al. (2019), using the NCI "Temperature-Flux" model. DePaolo et al. (2019) proposed that the whole-rock Nd isotopic signatures of a suite of Lhasa-area granitic plutons could be used as a quantitative proxy for crustal thickness based on the degree of isotopic assimilation between juvenile mantle and old crust. They use the parameterized Temperature-Flux model to approximate crustal thickness of Gangdese granitoids emplaced before and after the onset of continental collision. They identify a systematic decrease in whole-rock ε_{Nd} from south to north, from $\varepsilon_{Nd} = +5$ adjacent to the ITS to $\varepsilon_{Nd} = -13$, 110 km to the north. For the purpose of their model, DePaolo et al. (2019) use 48 Ma as a lower limit age for precollisional granites based on the compilations of Zhu et al. (2017). In ≥48 Ma Lhasa block granites, their model suggests a 25-35 km-thick crust adjacent to the ITS which thickens rapidly to >45 km-thick approximately 100 km north of the ITS. The ε_{Nd} of "postcollisional" granites (<32 Ma as defined by DePaolo et al., 2019) show evidence of a much thicker crust within ~50 km of the ITS; the crust was up to 75 km-thick adjacent to the suture by the latest Paleogene. The results of DePaolo et al. (2019) can be compared to patterns in zircon ε_{Hf}, age, and distance to the ITS, given similar behavior between Nd and Hf isotopic systems in crustal processes.

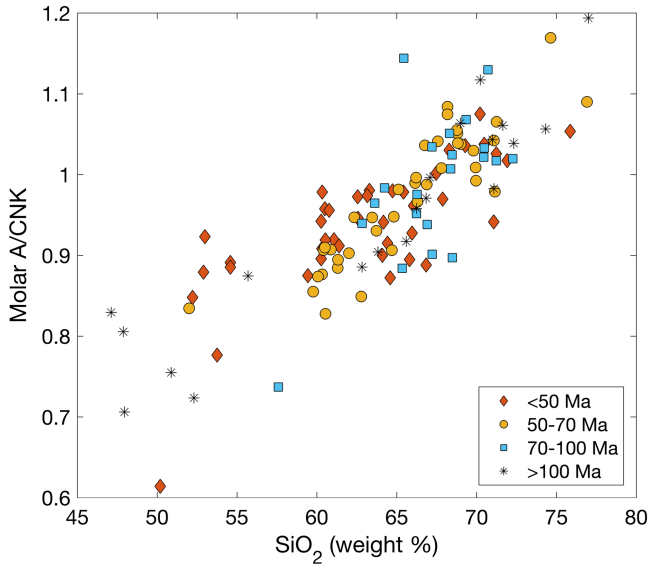

Figure 8. A/CNK = Molar $Al_2O_3/(CaO + Na_2O + K_2O)$ for granitoid samples (>60% SiO_2) and mafic enclaves (<60% SiO_2), representing typical fractional crystallization from a metaluminous mafic source; this pattern is unchanged from precollisional samples to later-syncollisional samples (< 50 Ma).

The isotopic data from this study are largely from locations farther east than those of DePaolo et al. (2019). Nevertheless, the equivalent north-south trend in both whole-rock and zircon ε_{Hf} reported here suggest the early syncollisional (48 Ma) structure inferred from the Nd data by DePaolo et al. (2019) extends to the east at least to 92.5° E, and that the two isotopic systems have preserved evidence of the same tectono-magmatic history of the region (Figure 4). Given the strong correlation between whole-rock and zircon ε_{Hf} (Figure 5), the latter may be used in conjunction with U-Pb ages to track the

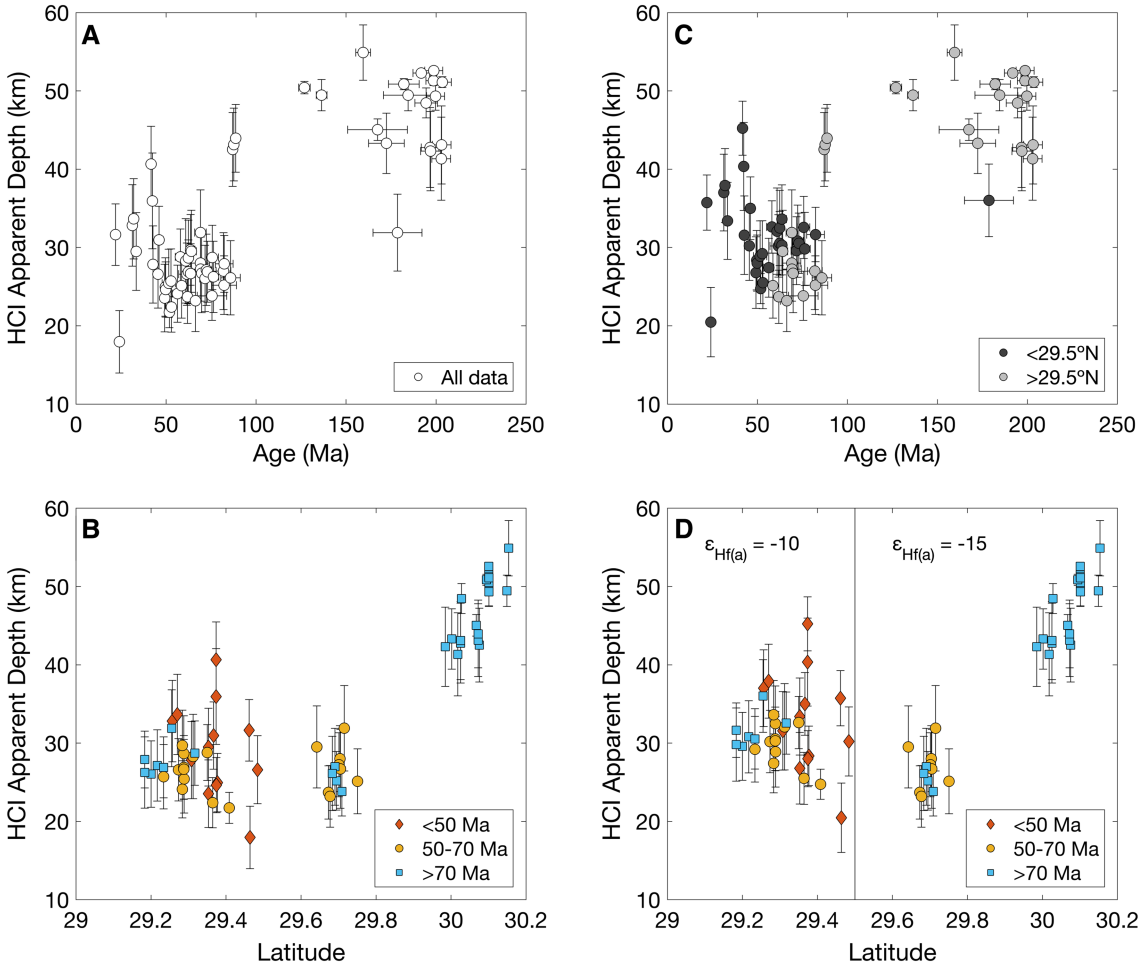

Figure 9. Zircon Hafnium Crustal Index ("HCI") apparent Moho depths with age (a,c) and latitude, sorted by age (b,d). Depths calculated from zircon HCI, assuming DM ε_{Hf} = +18 and crustal ε_{Hf} = -15 (b); crustal ε_{Hf} = -10 for samples south of 29.5°N (d) . Depth calculation using Temperature-Flux model of DePaolo et al. (2019) using similar parameters, such that depth $H = 2.4 + 80.6(HCI) - 29(HCI)^2$. Error bars on HCI derive from 2 s.e. of zircon Hf measurements. Age error bars are 2 s.e.

spatiotemporal evolution of the S. Tibetan crust. Though it is likely that initial collision began earlier than 50 Ma and gradually propagated to encompass the entire northern margin of India over the course of many Ma, reconstructed isotopic assimilation signatures as calculated by DePaolo et al. (2019) suggest that substantial changes in petrogenesis of Gangdese granites do not appear until <50 Ma; younger granites are treated here as "later-syncollisional" as a reflection of ongoing full continental collision from ~50 Ma to the present. The Hf isotopic data presented here represent samples aged 225±15 Ma to 22±1 Ma; only four units in our study fall within the <32 Ma criteria used by DePaolo et al. (2019) to infer later syncollisional thickening.

Using zircon Hf values as a basis, we applied the Temperature-Flux model to calculate NCI; herein we refer to it as "HCI": Hafnium Crustal Index (Figure 9). $\varepsilon_{Hf(r)}$ = +18 was used for the juvenile mantle value (Vervoort & Blichert-Toft, 1999). For the case of a latitudinally homogeneous crustal assimilant, we use $\varepsilon_{Hf(a)}$ = -15 as the endmember, consistent with a typically Proterozoic Tibetan basement (Zhu et al., 2011) (Figure 9a-b). HCI ranges from ~0.2 to 1, implying relatively high degrees of assimilation for all samples. Based on inherited zircon ε_{Hf} values presented in Zhu et al. (2011) and our pre-batholithic schist analyses, however, it is more likely that the crustal assimilant values are dependent on latitude. Recalculating HCI based on $\varepsilon_{Hf(a)}$ = -10 for samples south of 29.6°N and $\varepsilon_{Hf(a)}$ = -15 north of 29.6° leads to commensurately higher HCI for the southern samples. Using the Temperature-Flux model of DePaolo et al. (2019) with identical parameters, apparent crustal thicknesses range from ~18 km to ~55 km when $\varepsilon_{Hf(a)}$ = -15 for all samples. When samples south of 29.6° have $\varepsilon_{Hf(a)}$ = -10, the range is ~20 km to 55 km. Using the model

geotherm of DePaolo et al. (2019), HCI apparent depth increases within a narrow range of variations in sample ε_{Hf} until their values approach the composition of the crustal assimilant. An extremely steep model geotherm of 50°C/km forces a steeper association with HCI and depth, though such a steep geotherm would be unrealistically high for a typical arc setting, especially for depths greater than ~15 km (Rothstein & Manning, 2003). The assumption of $\varepsilon_{Hf(r)} = +18$ may be an overestimate, as the lithospheric mantle below the Tibetan crust may not be as depleted as global MORB or may have interacted with unradiogenic contaminant prior to melting and forming the magmas of interest, though the metavolcanic sample with $\varepsilon_{Hf} = +13$ suggests the lithospheric mantle under southern Lhasa was near to modern DM Hf composition. A more negative $\varepsilon_{Hf(r)}$ would lead to apparently thinner crust using the HCI Temperature-Flux model.

Calculated apparent depths can be associated with sample age (Figure 9a) and latitude (Figure 9b). When compared to age alone, HCI Moho depths imply a thinning crust between ~100 and 50 Ma, and a thickening crust following 50 Ma, though the spatial variations with latitude are obscured with this simple comparison. There is a clear discontinuity at ~29.8°N in precollisional samples in whole-rock ε_{Nd} and zircon ε_{Hf} (Figure 4a) which implies preexisting crustal structure that must be considered when evaluating relative thicknesses through time. Figure 9 shows little change from precollisional (> 70 Ma) to the early syncollisional period (50 – 70 Ma), and markedly increased apparent depths in later syncollisional samples near the ITS. The HCI results emulate the thickening inferred by DePaolo et al. (2019) from their ε_{Nd} – based Temperature-Flux model depths. Above an HCI of 1, corresponding to a Moho depth of ~55 km, our parameterization of the Temperature-Flux model saturates. That is, an HCI $\geq$ 1 implies 100% assimilation of the crustal component, and can therefore not be distinguished from isotopic assimilation occurring at greater depths. Cases where the apparent depth is $\geq$55 km represent this upper bound. For all syncollisional samples, however, the calculated HCI <1 implies these units formed within the limits of the model. The large range of HCI apparent Moho depths, especially among <50 Ma samples, could imply increased heterogeneity of the juvenile melt or the assimilant material, greater variation in the duration and volume of magma recharge during pluton construction, or may even betray inconsistencies in the assumed model parameters. It is possible the hybridization, assimilation, and crystallization environment of each individual sample was sufficiently different that applying the same model parameters to multiple samples obfuscates accurate calculation of HCI. Inferences may be drawn from systematic differences through time, regardless of depth accuracy, but the HCI model does not prove a priori whether the southern Tibetan crust was thick or thin prior to collision.

4.3. Structural Implications

The persistent gradient of positive, mantle-like zircon ε_{Hf} near the ITS, decreasing to more negative, evolved crustal signature to the north implies a strong controlling process on Hf isotopes in the Southern Lhasa Block for the past 200 Ma. Lack of deviation from strong mantle signature within ~ 80 km of the ITS in precollisional (> 50 Ma) and early syncollisional (40–50 Ma) plutons is additionally consistent with minimal assimilation of crustal material by a juvenile mantle melt source. Following the model of melt production occurring at the base of the crust, and degree of assimilation proportional to wall-rock temperature, minimal assimilation in all mid-Cretaceous to early Tertiary granites within ~80 km of the ITS implies granitic melt hybridization at the base of a thin crust, where country rock T was too low for substantial assimilation with juvenile melt. Increased heterogeneity in zircon ε_{Hf} of <50 Ma samples, all of which are found within 40 km of the ITS, supports this evidence of increased assimilation with crustal material, which in turn is consistent with higher-temperature storage and fractionation of these evolving melts. Accretion of subducted Indian upper-crustal material onto the base of the Eurasian crust at the ITS following the onset of continental collision would provide a new source of less radiogenic Hf at the base of the Eurasian crust; it would additionally contribute to the ongoing thickening process. A thickened Eurasian lower crust broadens the range of depths at which hybridized granitic melts would likely be emplaced, promoting additional heterogeneity in the degree of crustal assimilation for each discrete pluton (DePaolo, 1981; Kemp et al., 2007; Pearce, 1996).

The robust spatial trends in ε_{Nd} and ε_{Hf} as a function of N-S distance from the ITS must represent long-lived processes controlling the production and chemistry of the Gangdese batholith in the Lhasa block. There are three scenarios that could produce large volumes of granitic melt in Southern Tibet over many tens of Ma throughout the India-Asia collision: 1) Pure crustal anatexis of the (older) mid-crust in the

Lhasa block; 2) fractional crystallization of partial-melt of the mantle wedge; or 3) hybridization of juvenile mantle melt with crustal material at the Moho. Pure crustal anatexis is incapable of explaining the relatively homogeneous, mantle-like signature of both ε_{Hf} and $\delta^{18}O$ just prior to and during the early stages of collision. Jurassic granites in the central and northern Lhasa blocks have negative ε_{Hf} consistent with formation from melting of Proterozoic basement rocks with $^{176}Lu/^{177}Hf = 0.015$ (Zhu et al., 2011), with $\varepsilon_{Hf} \sim -15$; pre- and syncollisional melts forming from the same crustal root would be expected to have similarly negative ε_{Hf}.

Long-term maintenance of this regime of minimal assimilation at the ITS throughout the Jurassic and Cretaceous precludes major changes in the structure and crustal thickness of the southern Lhasa block throughout this time period. Despite the substantial magmatic inflation associated with the near-continuous emplacement of the Gangdese batholith during this period, there is no indication of significant precollisional crustal thickening, which would have resulted in greater degrees of crustal assimilation and anatexis in progressively younger rocks. The possibility that, in a thickened crust, younger Gangdese granites assimilated only with older mantle-derived Gangdese plutons (i.e., no crustal material), is precluded, as the Lhasa block bedrock includes substantial Cretaceous sedimentary strata (Kidd et al., 1988; Leier et al., 2007). An external process must therefore have controlled the geometry of the southern margin of the Lhasa block.

Prior to collision, the southern margin of the Lhasa block was a long-lived continental arc accommodating the closure of the neo-Tethys ocean basin (Allégre et al., 1984; Yin & Harrison, 2000). The crustal thickness at the arc margin, now the modern ITS, was a function of thickening due to magmatic inflation and tectonic accretion, and thinning due to erosion or exhumation (Lee et al., 2015). As the formation of the Gangdese batholith contributed to magmatic inflation of the Lhasa block, there must also have been continuous removal of crustal material at the ITS in order to maintain the wedge-shaped N-S geometry of the crust in southern Lhasa. Structural and paleoelevation studies of the Lhasa block (England & Searle, 1986; Ingalls et al., 2016; Murphy et al., 1997) suggest that the southern Tibetan plateau was at high elevation prior to continental collision (although England and Searle (1986) argued for precollisonal thickening occurring only in the Gangdese Batholith whereas our data suggest that the southernmost margin remained relatively thin until continental collision began).

The high convergence rate at the ITS prior to India-Asia continental collision (Rowley, 1996) and the evidence of steep subduction angle from ultra-high-pressure metamorphic rocks (Leech et al., 2005) suggest that moderate levels of subduction erosion may have controlled the thickness of the southern Tibetan crust without substantial input of slab material into the overriding plate. The rapid decrease in convergence rate, increase of subducted continental material, and flattening of the underriding slab following the onset of collision all would have contributed to increased addition of crustal material to syncollisional magmas, as observed in Hf, O, and Nd isotope systematics of syncollisional granitoids.

The HICLIMB study (Nábělek et al., 2009) imaged the Tibetan crust and upper mantle along a N-S transect about 150 km west of Lhasa. This 2D profile was interpreted as showing ~80 km thick crust across the block at this location, including ~35 km of Indian crust, although there are significant crustal thickness variations along strike (Zurek et al., 2007). Nábělek et al. (2009) interpreted anisotropy at the crust/mantle interface to reflect sustained shearing during formation. If this section is representative of the crustal structure beneath our transect then the lack of significant post-collisional upper crustal deformation in the southern Lhasa Block, as documented by the widespread unconformity between the Paleocene Linzizong Volcanics and Late Cretaceous Takena Formation (Dewey et al., 1988), and ~10 km of denudation adjacent the suture zone (e.g., Copeland et al., 1987) requires that ca. 50 km of crustal thickening has occurred since ~50 Ma (including the ~10 km lost via denudation) via accretion from below – most likely the result of underplating of Indian crust.

Four isotopic systems therefore are broadly consistent with the view that juvenile melts were hybridized and fractionated in the lower crust, with small degrees of crustal assimilation between ~90 to 50 Ma. Post-50 Ma samples at the ITS show greater degree of crustal assimilation, suggesting rapid thickening of the crust adjacent to the ITS since the onset of collision, which is consistent with interpretations of modern seismic data. In general agreement with results of recent geochemical models (DePaolo et al., 2019; Zhu et al., 2017), we infer that the southern margin of Tibet was relatively thin for at least 150 Ma prior to the onset of collision at ~50 Ma, and underwent rapid crustal thickening for at least the next 25 Ma.

5. Conclusions

A suite of Gangdese granites from a north-south transect around ~92°E in the Lhasa block of southern Tibet show significant north-south variation in Hf isotopes with distance from the southern margin of the Lhasa block, at the Indus-Tsangpo Suture (ITS). There is a strong correlation between zircon and whole-rock ε_{Hf} in units spanning >200 Ma to <40 Ma, permitting the use of zircon as a proxy for whole-rock ε_{Hf} in pre- and syncollisional plutons. Northward distance from the ITS is negatively correlated with zircon ε_{Hf}, with less radiogenic values in older, northward granites, while the bulk of <100 Ma granites within ~75 km of the ITS show more radiogenic, near mantle-like values. Whole-rock major element geochemistry, zircon ε_{Hf} and $\delta^{18}O$ of 50–180 Ma granites are consistent with continuous juvenile magma input to the lower crust of the southern margin of Tibet for the past ~200 Ma. Lack of heterogeneity in ITS-adjacent precollisional samples is consistent with low degrees of crustal assimilation during fractionation and emplacement of granitic magmas in the southern Lhasa block throughout the Jurassic and Cretaceous periods. Syncollisional (<50 Ma) samples show increasing geochemical evidence of assimilation with crustal material, both in greater heterogeneity of zircon ε_{Hf} as well as whole-rock major and trace element evidence (this study; Chen et al., 2018). Minimal precollisional crustal assimilation, and increased syncollisional assimilation in granites formed near the ITS is consistent with thermoisotopic modeling of whole-rock ε_{Nd} that indicates progressive thickening of the crust immediately adjacent to the ITS between ~50 and 32 Ma. Zircon U-Pb, Hf, and O isotopes, as well as whole-rock Hf isotopes and bulk geochemistry, indicate that the southern margin of the Lhasa block was thin for up to 150 Ma prior to collision, and thickened rapidly following the onset of hard collision at ~50 Ma. The persistence of calc-alkaline, mantle-like granitic melts throughout the lifetime of the precollisional continental arc is consistent with a wedge-shaped crustal geometry of the southern margin of the Lhasa block for 150 Ma prior to collision.

Acknowledgments
The authors acknowledge NSF grant EAR 1111586 for support of this research. The ion microprobe laboratory at UCLA is partially funded by a grant from NSF-EAR's Instrumentation and Facilities Program. The authors thank the two anonymous reviewers whose feedback helped improve the manuscript. The authors declare no financial conflicts of interest. Data has been submitted to be archived in EarthChem (https://doi.org/10.1594/IEDA/111402) and is also available in Supporting Information Tables S1 and S2.

References

Aikman, A. (2007). Tectonics of thse eastern Tethyan Himalaya, (Doctoral Dissertation). Retrieved from Open Research. (https://open-research-repository.anu.edu.au/handle/1885/146541) Canberra, Australia: Australian National University.

Allégre, C. J., Courtillot, V., Tapponnier, P., Hirn, A., Mattauer, M., Coulon, C., et al. (1984). Structure and evolution of the Himalaya–Tibet orogenic belt. *Nature*, *307*(5946), 17–22. https://doi.org/10.1038/307017a0

Bell, E. A., Harrison, T. M., McCulloch, M. T., & Young, E. D. (2011). Early Archean crustal evolution of the Jack Hills Zircon source terrane inferred from Lu–Hf, $^{207}Pb/^{206}Pb$, and $\delta^{18}O$ systematics of Jack Hills zircons. *Geochimica et Cosmochimica Acta*, *75*(17), 4816–4829. https://doi.org/10.1016/j.gca.2011.06.007

Bindeman, I. (2008). Oxygen Isotopes in Mantle and Crustal Magmas as Revealed by Single Crystal Analysis. *Reviews in Mineralogy and Geochemistry*, *69*(1), 445–478. https://doi.org/10.2138/rmg.2008.69.12

Blattner, P., Abart, R., Adams, C. J., Faure, K., & Hui, L. (2002). Oxygen isotope trends and anomalies in granitoids of the Tibetan plateau. *Journal of Asian Earth Sciences*, *21*(3), 241–250. https://doi.org/10.1016/S1367-9120(02)00046-9

Booth, A. L., Kolodny, Y., Chamberlain, C. P., McWilliams, M., Schmitt, A. K., & Wooden, J. (2005). Oxygen isotopic composition and U-Pb discordance in zircon. *Geochimica et Cosmochimica Acta*, *69*(20), 4895–4905. https://doi.org/10.1016/j.gca.2005.05.013

Bouilhol, P., Magni, V., van Hunen, J., & Kaislaniemi, L. (2015). A numerical approach to melting in warm subduction zones. *Earth and Planetary Science Letters*, *411*, 37–44. https://doi.org/10.1016/j.epsl.2014.11.043

Chapman, J. B., Ducea, M. N., Kapp, P., Gehrels, G. E., & DeCelles, P. G. (2017). Spatial and temporal radiogenic isotopic trends of magmatism in Cordilleran orogens. *Gondwana Research*, *48*, 189–204. https://doi.org/10.1016/j.gr.2017.04.019

Chapman, J. B., & Kapp, P. (2017). Tibetan Magmatism Database. *Geochemistry, Geophysics, Geosystems*, *18*, 4229–4234. https://doi.org/10.1002/2017GC007217

Chen, J. L., Yin, A., Xu, J. F., Dong, Y. H., & Kang, Z. Q. (2018). Late Cenozoic magmatic inflation, crustal thickening, and >2 km of surface uplift in central Tibet. *Geology*, *46*(1), 19–22. https://doi.org/10.1130/G39699.1

Chen, Y., Zhu, D. C., Zhao, Z. D., Meng, F. Y., Wang, Q., Santosh, M., et al. (2014). Slab breakoff triggered ca. 113Ma magmatism around Xainza area of the Lhasa Terrane, Tibet. *Gondwana Research*, *26*(2), 449–463. https://doi.org/10.1016/j.gr.2013.06.005

Chung, S. L., Chu, M. F., Ji, J., O'Reilly, S. Y., Pearson, N. J., Liu, D., et al. (2009). The nature and timing of crustal thickening in Southern Tibet: Geochemical and zircon Hf isotopic constraints from postcollisional adakites. *Tectonophysics*, *477*(1-2), 36–48. https://doi.org/10.1016/j.tecto.2009.08.008

Chung, S.-L., Chu, M.-F., Zhang, Y., Xie, Y., Lo, C.-H., Lee, T.-Y.,et al. (2005). Tibetan tectonic evolution inferred from spatial and temporal variations in post-collisional magmatism. *Earth-Science Reviews*, *68*(3–4), 173–196. https://doi.org/10.1016/j.earscirev.2004.05.001

Copeland, P., Harrison, T. M., Kidd, W. S. F., Xu, R., & Zhan, Y. (1987). Rapid early Miocene acceleration of uplift in the Gangdese Belt, Xizang (southern Tibet), and its bearing on accommodation mechanisms of the India-Asia collision. *Earth and Planetary Science Letters*, *86*(2), 240–252. https://doi.org/10.1016/0012-821X(87)90224-X

De Yoreo, J. J., Lux, D. R., & Guidotti, C. V. (1989). The role of crustal anatexis and magma migration in the thermal evolution of regions of thickened continental crust. *Geological Society, London, Special Publications*, *43*(1), 187–202. https://doi.org/10.1144/GSL.SP.1989.043.01.12

DePaolo, D. J., Harrison, T. M., Wielicki, M., Zhao, Z. D., Zhu, D. C., Zhang, H., & Mo, X. X. (2019). Geochemical evidence for thin syn-collision crust and major crustal thickening between 45 and 32 Ma at the southern margin of Tibet. *Gondwana Research*, *73*, 123–135. https://doi.org/10.1016/j.gr.2019.03.011

DePaolo, D. J. (1981). Trace element and isotopic effects of combined wallrock assimilation and fractional crystallization. *Earth and Planetary Science Letters*, *53*(2), 189–202. https://doi.org/10.1016/0012-821X(81)90153-9

DePaolo, D. J., Perry, F. V., & Baldridge, W. S. (1992). Crustal versus mantle sources of granitic magmas: a two-parameter model based on Nd isotopic studies. *Earth and Environmental Science Transactions of The Royal Society of Edinburgh*, *83*(1–2), 439–446. https://doi.org/10.1017/S0263593300008117

Dewey, J. F., Shackleton, R. M., Chang, C. F., & Sun, Y. Y. (1988). The tectonic evolution of the Tibetan Plateau. *Philosophical Transactions of the Royal Society of London. Series A, Mathematical and Physical Sciences*, *327*(1594), 379–413. https://doi.org/10.1098/rsta.1988.0135

Eiler, J. M. (2001). Oxygen Isotope Variations of Basaltic Lavas and Upper Mantle Rocks. *Reviews in Mineralogy and Geochemistry*, *43*(1), 319–364. https://doi.org/10.2138/gsrmg.43.1.319

England, P., & Houseman, G. (1986). Finite strain calculations of continental deformation: 2. Comparison with the India-Asia Collision Zone. *Journal of Geophysical Research*, *91*(B3), 3664–3676. https://doi.org/10.1029/JB091iB03p03664

England, P., & McKenzie, D. (1982). A thin viscous sheet model for continental deformation. *Geophysical Journal of the Royal Astronomical Society*, *70*(2), 295–321. https://doi.org/10.1111/j.1365-246X.1982.tb04969.x

England, P., & Searle, M. (1986). The Cretaceous-tertiary deformation of the Lhasa Block and its implications for crustal thickening in Tibet. *Tectonics*, *5*(1), 1–14. https://doi.org/10.1029/TC005i001p00001

Ferry, J. M., & Watson, E. B. (2007). New thermodynamic models and revised calibrations for the Ti-in-zircon and Zr-in-rutile thermometers. *Contributions to Mineralogy and Petrology*, *154*(4), 429–437. https://doi.org/10.1007/s00410-007-0201-0

Finch, R. J., & Hanchar, J. M. (2003). Structure and Chemistry of Zircon and Zircon-Group Minerals. *Reviews in Mineralogy and Geochemistry*, *53*(1), 1–25. https://doi.org/10.2113/0530001

Garzanti, E., Radeff, G., & Malusà, M. G. (2018). Slab breakoff: A critical appraisal of a geological theory as applied in space and time. *Earth-Science Reviews*, *177*, 303–319. https://doi.org/10.1016/j.earscirev.2017.11.012

Gregory, R. T., & Taylor, H. P. (1981). An oxygen isotope profile in a section of Cretaceous oceanic crust, Samail Ophiolite, Oman: Evidence for $\delta^{18}O$ buffering of the oceans by deep (>5 km) seawater-hydrothermal circulation at mid-ocean ridges. *Journal of Geophysical Research*, *86*(B4), 2737–2755. https://doi.org/10.1029/JB086iB04p02737

Hammersley, L., & DePaolo, D. J. (2006). Isotopic and geophysical constraints on the structure and evolution of the Clear Lake volcanic system. *Journal of Volcanology and Geothermal Research*, *153*(3–4), 331–356. https://doi.org/10.1016/j.jvolgeores.2005.12.003

Harrison, T. M., Copeland, P., Kidd, W. S. F., & Yin, A. (1992). Raising Tibet. *Science*, *255*(5052), 1663–1670. https://doi.org/10.1126/science.255.5052.1663

Harrison, T. M., Schmitt, A. K., McCulloch, M. T., & Lovera, O. M. (2008). Early (≥4.5 Ga) formation of terrestrial crust: Lu–Hf, $\delta^{18}O$, and Ti thermometry results for Hadean zircons. *Earth and Planetary Science Letters*, *268*(3), 476–486. https://doi.org/10.1016/j.epsl.2008.02.011

Harrison, T. M., Wielicki, M. M., Lovera, O. M., DePaolo, D. J., Zhu, D. C., Zhao, Z., Yin, A., & Mo, X. (2014). *Testing tectonic models using time-varying crustal thickness variations across Southern Tibet. Paper presented at GSA Annual Meeting*. B.C.: Vancouver.

Harrison, T. M., Yin, A., Grove, M., Lovera, O. M., Ryerson, F. J., & Zhou, X. (2000). The Zedong Window: A record of superposed Tertiary convergence in southeastern Tibet. *Journal of Geophysical Research*, *105*(B8), 19,211–19,230. https://doi.org/10.1029/2000JB900078

Houseman, G. A., McKenzie, D. P., & Molnar, P. (1981). Convective instability of a thickened boundary layer and its relevance for the thermal evolution of continental convergent belts. *Journal of Geophysical Research*, *86*(B7), 6115–6132. https://doi.org/10.1029/JB086iB07p06115

Ingalls, M., Rowley, D. B., Currie, B., & Colman, A. S. (2016). Large-scale subduction of continental crust implied by India–Asia mass-balance calculation. *Nature Geoscience*, *9*(11), 848. https://doi.org/10.1038/ngeo2806

Ito, E., White, W. M., & Göpel, C. (1987). The O, Sr, Nd and Pb isotope geochemistry of MORB. *Chemical Geology*, *62*(3), 157–176. https://doi.org/10.1016/0009-2541(87)90083-0

Ji, W. Q., Wu, F. Y., Chung, S. L., Li, J. X., & Liu, C. Z. (2009). Zircon U–Pb geochronology and Hf isotopic constraints on petrogenesis of the Gangdese batholith, southern Tibet. *Chemical Geology*, *262*(3), 229–245. https://doi.org/10.1016/j.chemgeo.2009.01.020

Ji, W. Q., Wu, F. Y., Chung, S. L., Wang, X. C., Liu, C. Z., Li, Q. L., et al. (2016). Eocene Neo-Tethyan slab breakoff constrained by 45 Ma oceanic island basalt–type magmatism in southern Tibet. *Geology*, *44*(4), 283–286. https://doi.org/10.1130/G37612.1

Jochum, K., Weis, U., Stoll, B., Kuzmin, D., Yang, Q., Raczek, I., et al. (2011). Determination of reference values for NIST SRM 610–617 glasses following ISO Guidelines. *Geostandards and Geoanalytical Research*, *35*(4), 397–429. https://doi.org/10.1111/j.1751-908X.2011.00120.x

Johnson, D. M., Hooper, P. R., & Conrey, R. M. (1999). XRF Analysis of Rocks and Minerals for Major and Trace Elements on a Single Low Dilution Li-tetraborate Fused Bead. *Advances in X-Ray Analysis*, *41*, 843–867.

Johnson, M. R. W. (2002). Shortening budgets and the role of continental subduction during the India-Asia collision. *Earth-Science Reviews*, *59*(1-4), 101–123.

Kapp, J. L. D., Harrison, T. M., Kapp, P., Grove, M., Lovera, O. M., & Lin, D. (2005). Nyainqentanglha Shan: A window into the tectonic, thermal, and geochemical evolution of the Lhasa block, southern Tibet. *Journal of Geophysical Research*, *110*, B08413. https://doi.org/10.1029/2004JB003330

Kapp, P., Manning, C. E., & Tropper, P. (2009). Phase-equilibrium constraints on titanite and rutile activities in mafic epidote amphibolites and geobarometry using titanite–rutile equilibria. *Journal of Metamorphic Geology*, *27*(7), 509–521. https://doi.org/10.1111/j.1525-1314.2009.00836.x

Kemp, A. I. S., Hawkesworth, C. J., Foster, G. L., Paterson, B. A., Woodhead, J. D., Hergt, J. M., et al. (2007). Magmatic and Crustal Differentiation History of Granitic Rocks from Hf-O Isotopes in Zircon. *Science*, *315*(5814), 980–983. https://doi.org/10.1126/science.1136154

Kidd, W. S. F., Yusheng, P., Chengfa, C., Coward, M. P., Dewey, J. F., Gansser, A., et al. (1988). Geological mapping of the 1985 Chinese—British Tibetan (Xizang—Qinghai) Plateau Geotraverse route. *Philosophical Transactions of the Royal Society of London. Series A, Mathematical and Physical Sciences*, *327*(1594), 287–305. https://doi.org/10.1098/rsta.1988.0130

King, E. M., Barrie, C. T., & Valley, J. W. (1997). Hydrothermal alteration of oxygen isotope ratios in quartz phenocrysts, Kidd Creek mine, Ontario: Magmatic values are preserved in zircon. *Geology*, *25*(12), 1079–1082. https://doi.org/10.1130/0091-7613(1997)025<1079:HAOOIR>2.3.CO;2

Kinny, P. D., & Maas, R. (2003). Lu–Hf and Sm–Nd isotope systems in zircon. *Reviews in Mineralogy and Geochemistry*, *53*(1), 327–341. https://doi.org/10.2113/0530327

Klaver, M., Blundy, J. D., & Vroon, P. Z. (2018). Generation of arc rhyodacites through cumulate-melt reactions in a deep crustal hot zone: Evidence from Nisyros volcano. *Earth and Planetary Science Letters*, *497*, 169–180. https://doi.org/10.1016/j.epsl.2018.06.019

Kong, X., & Bird, P. (1995). SHELLS: A thin-shell program for modeling neotectonics of regional or global lithosphere with faults. *Journal of Geophysical Research*, *100*(B11), 22,129–22,131. https://doi.org/10.1029/95JB02435

Kong, X., Yin, A., & Harrison, T. M. (1997). Evaluating the role of preexisting weaknesses and topographic distributions in the Indo-Asian collision by use of a thin-shell numerical model. *Geology*, *25*(6), 527–530. https://doi.org/10.1130/0091-7613(1997)025<0527:ETROPW>2.3.CO;2

Lackey, J. S., Cecil, M. R., Windham, C. J., Frazer, R. E., Bindeman, I. N., & Gehrels, G. E. (2012). The Fine Gold Intrusive Suite: The roles of basement terranes and magma source development in the Early Cretaceous Sierra Nevada batholith. *Geosphere*, *8*(2), 292–313. https://doi.org/10.1130/GES00745.1

Le Fort, P. (1996). Evolution of the Himalaya. In T. M. Harrison, & A. Yin (Eds.), *The Tectonics of Asia*, (pp. 95–106). Cambridge University Press.

Lee, C. T. A., Thurner, S., Paterson, S., & Cao, W. (2015). The rise and fall of continental arcs: Interplays between magmatism, uplift, weathering, and climate. *Earth and Planetary Science Letters*, *425*, 105–119. https://doi.org/10.1016/j.epsl.2015.05.045

Leech, M. L., Singh, S., Jain, A. K., Klemperer, S. L., & Manickavasagam, R. M. (2005). The onset of India–Asia continental collision: Early, steep subduction required by the timing of UHP metamorphism in the western Himalaya. *Earth and Planetary Science Letters*, *234*(1), 83–97. https://doi.org/10.1016/j.epsl.2005.02.038

Leier, A. L., Kapp, P., Gehrels, G. E., & DeCelles, P. G. (2007). Detrital zircon geochronology of Carboniferous–Cretaceous strata in the Lhasa terrane, Southern Tibet. *Basin Research*, *19*(3), 361–378. https://doi.org/10.1111/j.1365-2117.2007.00330.x

Lovera, O. M., Harrison, M., Schmitt, A. K., Wielicki, M. M., & Tierney, C. R. (2015). Numerical Simulation of Magma Reservoirs to Interpret Chrono-Chemical Signal. Paper presented at the AGU Fall Meeting, San Francisco, CA.

McNulty, B. A., Tobisch, O. T., Cruden, A. R., & Gilder, S. (2000). Multistage emplacement of the Mount Givens pluton, central Sierra Nevada batholith, California. *GSA Bulletin*, *112*(1), 119–135. https://doi.org/10.1130/0016-7606(2000)112<119:MEOTMG>2.0.CO;2

Mo, X. X., Dong, G., Zhao, Z. D., Zhou, S., Wang, L. L., Qiu, R. Z., & Zhang, F. Q. (2005). Spatial and temporal distribution and characteristics of granitoids in the Gangdese, Tibet and implication for crustal growth and evolution. *Geological Journal of China Universities*, *11*(3), 281–290.

Mo, X. X., Hou, Z., Niu, Y., Dong, G., Qu, X., Zhao, Z., & Yang, Z. (2007). Mantle contributions to crustal thickening during continental collision: evidence from Cenozoic igneous rocks in southern Tibet. *Lithos*, *96*(1-2), 225–242.

Mojzsis, S. J., Harrison, T. M., & Pidgeon, R. T. (2001). Oxygen-isotope evidence from ancient zircons for liquid water at the Earth's surface 4,300 Myr ago. *Nature*, *409*(6817), 178–181. https://doi.org/10.1038/35051557

Mungall, J. E., Dingwell, D. B., & Chaussidon, M. (1999). Chemical diffusivities of 18 trace elements in granitoid melts. *Geochimica et Cosmochimica Acta*, *63*(17), 2599–2610. https://doi.org/10.1016/s0016-7037(99)00209-4

Murphy, M. A., Yin, A., Harrison, T. M., Durr, S. B., Ryerson, F. J., & Kidd, W. S. F. (1997). Did the Indo-Asian collision alone create the Tibetan plateau? *Geology*, *25*(8), 719–722. https://doi.org/10.1130/0091-7613(1997)025<0719:DTIACA>2.3.CO;2

Nábělek, J., Hetényi, G., Vergne, J., Sapkota, S., Kafle, B., Jiang, M., et al. (2009). Underplating in the Himalaya-Tibet Collision Zone Revealed by the Hi-CLIMB Experiment. *Science*, *325*(5946), 1371–1374. https://doi.org/10.1126/science.1167719

Paces, J. B., & Miller, J. D. (1993). Precise U-Pb ages of Duluth Complex and related mafic intrusions, northeastern Minnesota: Geochronological insights to physical, petrogenetic, paleomagnetic, and tectonomagmatic processes associated with the 1.1 Ga Midcontinent Rift System. *Journal of Geophysical Research*, *98*(B8), 13,997–14,013. https://doi.org/10.1029/93JB01159

Patchett, P. J., Kouvo, O., Hedge, C. E., & Tatsumoto, M. (1982). Evolution of continental crust and mantle heterogeneity: Evidence from Hf isotopes. *Contributions to Mineralogy and Petrology*, *78*(3), 279–297. https://doi.org/10.1007/BF00398923

Pearce, J. A. (1996). Sources and settings of granitic rocks. *Episodes*, *19*(4), 120–125. https://doi.org/10.1111/j.1751-908X.2011.00120.x

Peltzer, G., & Saucier, F. (1996). Present-day kinematics of Asia derived from geologic fault rates. *Journal of Geophysical Research*, *101*(B12), 27943–27956. https://doi.org/10.1029/96JB02698

Peltzer, G., & Tapponnier, P. (1988). Formation and evolution of strike-slip faults, rifts, and basins during the India-Asia Collision: An experimental approach. *Journal of Geophysical Research*, *93*(B12), 15,085–15,117. https://doi.org/10.1029/JB093iB12p15085

Quidelleur, X., Grove, M., Lovera, O. M., Harrison, T. M., Yin, A., & Ryerson, F. J. (1997). Thermal evolution and slip history of the Renbu Zedong Thrust, southeastern Tibet. *Journal of Geophysical Research*, *102*(B2), 2659–2679. https://doi.org/10.1029/96JB02483

Rapp, R. P., Shimizu, N., & Norman, M. D. (2003). Growth of early continental crust by partial melting of eclogite. *Nature*, *425*(6958), 605–609. https://doi.org/10.1038/nature02031

Reiners, P. W., Nelson, B. K., & Ghiorso, M. S. (1995). Assimilation of felsic crust by basaltic magma: Thermal limits and extents of crustal contamination of mantle-derived magmas. *Geology*, *23*(6), 563–566. https://doi.org/10.1130/0091-7613(1995)023<0563:AOFCBB>2.3.CO;2

Rothstein, D. A., & Manning, C. E. (2003). Geothermal gradients in continental magmatic arcs: Constraints from the eastern Peninsular Ranges batholith, Baja California, México. In Tectonic Evolution of Northwestern México and the Southwestern USA (Vol. 374). Geological Society of America.

Rowley, D. B. (1996). Age of initiation of collision between India and Asia: A review of stratigraphic data. *Earth and Planetary Science Letters*, *145*(1), 1–13. https://doi.org/10.1016/S0012-821X(96)00201-4

Simon, J. I., Weis, D., DePaolo, D. J., Renne, P. R., Mundil, R., & Schmitt, A. K. (2014). Assimilation of preexisting Pleistocene intrusions at Long Valley by periodic magma recharge accelerates rhyolite generation: rethinking the remelting model. *Contributions to Mineralogy and Petrology*, *167*(1), 1–34. https://doi.org/10.1007/s00410-013-0955-5

Spera, F. J., & Bohrson, W. A. (2002). Energy-constrained open-system magmatic processes 3. Energy-Constrained Recharge, Assimilation, and Fractional Crystallization (EC-RAFC). *Geochemistry, Geophysics, Geosystems*, *3*(12), 8001. https://doi.org/10.1029/2002gc000315

Tapponnier, P., Peltzer, G., Le Dain, A. Y., Armijo, R., & Cobbold, P. (1982). Propagating extrusion tectonics in Asia: New insights from simple experiments with plasticine. *Geology*, *10*(12), 611. https://doi.org/10.1130/0091-7613(1982)102.0.co;2

Trail, D., Bindeman, I. N., Watson, E. B., & Schmitt, A. K. (2009). Experimental calibration of oxygen isotope fractionation between quartz and zircon. *Geochimica et Cosmochimica Acta*, *73*(23), 7110–7126. https://doi.org/10.1016/j.gca.2009.08.024

Trail, D., Mojzsis, S. J., Harrison, T. M., Schmitt, A. K., Watson, E. B., & Young, E. D. (2007). Constraints on Hadean zircon protoliths from oxygen isotopes, Ti-thermometry, and rare earth elements. *Geochemistry, Geophysics, Geosystems*, *8*, Q06014. https://doi.org/10.1029/2006GC001449

Valley, J. W. (2003). Oxygen Isotopes in Zircon. *Reviews in Mineralogy and Geochemistry*, *53*(1), 343–385. https://doi.org/10.2113/0530343

Vervoort, J. D., & Blichert-Toft, J. (1999). Evolution of the depleted mantle: Hf isotope evidence from juvenile rocks through time. *Geochimica et Cosmochimica Acta*, *63*(3), 533–556. https://doi.org/10.1016/S0016-7037(98)00274-9

Walker, B. A., Miller, C. F., Lowery Claiborne, L., Wooden, J. L., & Miller, J. S. (2007). Geology and geochronology of the Spirit Mountain batholith, southern Nevada: Implications for timescales and physical processes of batholith construction. *Journal of Volcanology and Geothermal Research*, *167*(1), 239–262. https://doi.org/10.1016/j.jvolgeores.2006.12.008

Watson, E. B., & Cherniak, D. J. (1997). Oxygen diffusion in zircon. *Earth and Planetary Science Letters*, *148*(3), 527–544. https://doi.org/10.1016/S0012-821X(97)00057-5

Weis, D., Kieffer, B., Hanano, D., Nobre Silva, I., Barling, J., Pretorius, W., et al. (2007). Hf isotope compositions of U.S. Geological Survey reference materials. *Geochemistry, Geophysics, Geosystems*, *8*, Q06006. https://doi.org/10.1029/2006GC001473

Wiebe, R. A., & Collins, W. J. (1998). Depositional features and stratigraphic sections in granitic plutons: implications for the emplacement and crystallization of granitic magma. *Journal of Structural Geology*, *20*(9), 1273–1289. https://doi.org/10.1016/S0191-8141(98)00059-5

Wiedenbeck, M., Hanchar, J. M., Peck, W. H., Sylvester, P., Valley, J., Whitehouse, M., et al. (2004). Further Characterization of the 91500 Zircon Crystal. *Geostandards and Geoanalytical Research*, *28*(1), 9–39. https://doi.org/10.1111/j.1751-908X.2004.tb01041.x

Woodhead, J. D., & Hergt, J. M. (2005). A Preliminary Appraisal of Seven Natural Zircon Reference Materials for In Situ Hf Isotope Determination. *Geostandards and Geoanalytical Research*, *29*(2), 183–195. https://doi.org/10.1111/j.1751-908X.2005.tb00891.x

Yin, A., & Harrison, T. M. (2000). Geologic Evolution of the Himalayan-Tibetan Orogen. *Annual Review of Earth and Planetary Sciences*, *28*(1), 211–280. https://doi.org/10.1146/annurev.earth.28.1.211

York, D., Evensen, N. M., Martinez, M. L., & De Basabe, D. J. (2004). Unified equations for the slope, intercept, and standard errors of the best straight line. *American Journal of Physics*, *72*(3), 367–375. https://doi.org/10.1119/1.1632486

Zhang, Z., Dong, X., Xiang, H., Ding, H., He, Z., & Liou, J. G. (2015). Reworking of the Gangdese magmatic arc, southeastern Tibet: post-collisional metamorphism and anatexis. *Journal of Metamorphic Geology*, *33*(1), 1–21. https://doi.org/10.1111/jmg.12107

Zhu, D. C., Mo, X. X., Niu, Y., Zhao, Z. D., Wang, L. Q., Pan, G. T., & Wu, F. Y. (2009). Zircon U–Pb dating and in-situ Hf isotopic analysis of Permian peraluminous granite in the Lhasa terrane, southern Tibet: Implications for Permian collisional orogeny and paleogeography. *Tectonophysics*, *469*(1-4), 48–60. https://doi.org/10.1016/j.tecto.2009.01.017

Zhu, D. C., Wang, Q., Cawood, P. A., Zhao, Z. D., & Mo, X. X. (2017). Raising the Gangdese Mountains in southern Tibet. *Journal of Geophysical Research: Solid Earth*, *122*, 214–223. https://doi.org/10.1002/2016JB013508

Zhu, D. C., Wang, Q., Zhao, Z. D., Chung, S. L., Cawood, P. A., Niu, Y., et al. (2015). Magmatic record of India-Asia collision. *Scientific Reports*, *5*(1). https://doi.org/10.1038/srep14289

Zhu, D. C., Zhao, Z. D., Niu, Y., Mo, X. X., Chung, S. L., Hou, Z. Q., et al. (2011). The Lhasa Terrane: Record of a microcontinent and its histories of drift and growth. *Earth and Planetary Science Letters*, *301*(1-2), 241–255. https://doi.org/10.1016/j.epsl.2010.11.005

Zurek, B., Meltzer, A., & Sol, S. (2007). Metamorphism and deformation of the lower crust and crust-mantle interface at the eastern syntaxis of Tibet derived from converted seismic waves. T22C-05. Paper presented at the AGU Fall Meeting, San Francisco, CA.